

# Hilbert space and ground state structure of bilayer quantum Hall systems at $\nu = 2/\lambda$

M. Calixto, C. Peón-Nieto and E. Pérez-Romero

*Departamento de Matemática Aplicada and Instituto "Carlos I" de Física Teórica y Computacional,  
Universidad de Granada, Fuentenueva s/n, 18071 Granada, Spain*

(Dated: April 21, 2022)

We analyze the Hilbert space and ground state structure of bilayer quantum Hall (BLQH) systems at fractional filling factors  $\nu = 2/\lambda$  and we also study the large  $SU(4)$  isospin- $\lambda$  limit. The model Hamiltonian is an adaptation of the  $\nu = 2$  case [1] to the many-body situation (arbitrary  $\lambda$  flux quanta per electron). The semiclassical regime and quantum phase diagram (in terms of layer distance, Zeeman, tunneling, etc, control parameters) is obtained by using previously introduced Grassmannian  $\mathbb{G}_2^4 = U(4)/[U(2) \times U(2)]$  coherent states as variational states. The existence of three quantum phases (spin, canted and ppin) is common to any  $\lambda$ , but the phase transition points depend on  $\lambda$ , and the instance  $\lambda = 1$  is recovered as a particular case. We also analyze the quantum case through a numerical diagonalization of the Hamiltonian and compare with the mean-field results, which give a good approximation in the spin and ppin phases but not in the canted phase, where we detect exactly  $\lambda$  energy level crossings between the ground and first excited state for given values of the tunneling gap. An energy band structure at low and high interlayer tunneling (spin and ppin phases, respectively) also appears depending on angular momentum and layer population imbalance quantum numbers.

PACS numbers: 73.43.-f, 73.43.Nq, 73.43.Jn, 71.10.Pm, 03.65.Fd

## I. INTRODUCTION

A better analytical understanding of the Hilbert space and ground state structure of multicomponent fractional quantum Hall systems is needed to have a clear physical picture and to properly interpret the experimental data. In this article we make a contribution in this direction, studying the bilayer case at fractional values of the filling factor  $\nu = 2/\lambda$  and the limit  $\lambda \rightarrow \infty$ . According to Jain's composite fermion picture [2], this is the case of 2 quasiparticles (2 electrons bound to  $\lambda$  magnetic flux quanta each) per Landau site. The integer case  $\nu = 2$  has been extensively studied in the literature (see e.g. [1, 3–8]), where the analysis of the ground state structure reveals the existence of (in general) three quantum phases, shortly denoted by: spin, canted and ppin [1, 3], depending on which order parameter (spin or pseudospin/layer) dominates across the control parameter space: tunneling, Zeeman, bias, etc, couplings [see later on Eq. (14)]. The fractional multicomponent case (including multilayer, graphene, etc) has also been addressed (see e.g. [10–14]). In particular, for the bilayer quantum Hall (BLQH) system, the fractional case  $\nu = 2/3$  has been theoretically worked out in [15], having an excellent agreement with previous experimental results [16, 17].

The variational states used to study the ground state and phase diagrams of (multicomponent) fractional QH systems are usually of Laughlin [18] (phenomenological) type. Complementary descriptions are provided by Halperin [19] and Haldane's [20] scheme of hierarchy states, Jain's composite fermion theory [2], hierarchy states by MacDonald et al. [21], etc. In this article we shall use wave functions introduced previously by us in a series of papers, firstly for the bilayer case at frac-

tional values  $\nu = 2/\lambda$  [22–24] and recently extended to the  $N$ -component case at  $\nu = M/\lambda$  in [25]. We followed a group-theoretical approach that generalizes the classification of  $SU(4)$  isospin states at  $\nu = 2$  according to the 6-dimensional irreducible totally antisymmetric representation  $[1, 1]$  of  $SU(4)$  arising in the decomposition of  $4 \otimes 4 = 10 \oplus 6$ . For  $\nu = 2/\lambda$  we constructed the  $d_\lambda$ -dimensional (4) irreducible representation of  $SU(4)$  which, in Young tableau notation  $[\lambda, \lambda]$ , consists of two rows (two electrons) of  $\lambda$  boxes (flux quanta) each [see eq. (3)]. The corresponding phase space is the Grassmannian  $\mathbb{G}_2^4 = U(4)/[U(2) \times U(2)]$ , a picture that has also been considered in some extensions to  $N$ -component antiferromagnets [26–28]. The dimension  $d_\lambda$  of the corresponding Hilbert space grows as  $d_\lambda \sim \lambda^4$  (4) since there are more and more ways of attaching flux quanta to the indistinguishable electrons. These states have been used to quantify interlayer coherence and entanglement in the BLQH system at  $\nu = 2/\lambda$  [23]. Here we test our Grassmannian  $\mathbb{G}_2^4$  coherent states as variational states to study the quantum phase diagram (according to Gilmore's algorithm [29]) at filling factor  $\nu = 2/\lambda$ , the case  $\lambda = 1$  being recovered as a particular case [1, 3]. We shall see that the existence of the three quantum phases (spin, canted and ppin) is common to any  $\lambda$ , but the phase transition points depend on  $\lambda$ . We study the large isospin  $\lambda \rightarrow \infty$  limit and realize that the canted region shrinks for high values of  $\lambda$  in the tunneling direction. We also analyze the quantum case through a numerical diagonalization of the Hamiltonian and compare the results with the mean field (semiclassical) case. We obtain good agreement between quantum and semiclassical results in the spin and ppin phases, but not in the canted phase, where we detect exactly  $\lambda$  energy-level crossings between the ground and first excited states for given values of the tunneling gap. Therefore, this degeneracy problem becomes

more apparent for higher  $\lambda$ . The fidelity (overlap) between variational and numerical ground states increases when we adapt our coherent states to a parity symmetry, as turns out also to occur in other quantum physical systems undergoing a second order QPT like the Dicke model of atom-field interactions [30–32], vibron model of molecules [33–36], Lipkin-Meshkov-Glick [37], etc.

The organization of the paper is the following. In section II we provide an oscillator realization of the  $U(4)$  operators and the Landau-site Hilbert space for  $\nu = 2/\lambda$ , together with their matrix elements, which will be necessary for the quantum analysis addressed in section IV. More details can be found in references [22–24] and appendices A and B, which have been introduced for the sake of self-containedness. Specially appendix B, which contains the isospin- $\lambda$  coherent states, essential for the semiclassical analysis of the model Hamiltonian studied in section III. The Landau-site Hamiltonian governing the BLQH system at  $\nu = 2/\lambda$  is an adaptation of the one proposed in [1] for  $\lambda = 1$  to the many body case (arbitrary  $\lambda$ ). Using our coherent states, we obtain in section III the phase diagram (in the balanced case, for simplicity) for arbitrary  $\lambda$  and, in particular, we recover the results of [1] for  $\lambda = 1$ . We also study the large isospin  $\lambda \rightarrow \infty$  limit. In section IV we analyze the quantum case through a numerical diagonalization of the Hamiltonian and compare the results with the mean field (semiclassical) case. For low and high interlayer tunneling (spin and ppin phases, respectively) an analytical treatment of the Hamiltonian reveals a formation of energy bands depending on angular momentum and layer population imbalance quantum numbers. We study the internal structure of these bands (for other studies on band structure formation in the FQHE see e.g. [38]). The last section is left for conclusions and outlook.

## II. $U(4)$ OPERATORS AND HILBERT SPACE

BLQH systems underlie an isospin  $U(4)$  symmetry. In order to emphasize the spin  $SU(2)$  symmetry in the, let us say, bottom  $b$  (pseudospin down) and top  $a$  (pseudospin up) layers, it is customary to denote the  $U(4)$  generators in the four-dimensional fundamental representation by the sixteen  $4 \times 4$  matrices  $\tau_{\mu\nu} \equiv \sigma_{\mu}^{\text{ppin}} \otimes \sigma_{\nu}^{\text{spin}}$ ,  $\mu, \nu = 0, 1, 2, 3$ , where  $\sigma_{\mu}$  denote the usual Pauli matrices  $\sigma_k, k = 1, 2, 3$ , plus the identity  $\sigma_0$ . In the fractional case, bosonic magnetic flux quanta are attached to the electrons to form composite fermions. Let us denote by  $(a_l^{\downarrow})^{\dagger}$  [resp.  $(b_l^{\uparrow})^{\dagger}$ ] creation operators of magnetic flux quanta (flux quanta in the sequel) attached to the electron  $l$  with spin down [resp. up] at layer  $a$  [resp.  $b$ ], and so on. For the case of two electrons,  $l = 1, 2$ , the four-component electron “field”  $\mathcal{Z}$  is arranged as a compound  $\mathcal{Z} = (\mathcal{Z}_1, \mathcal{Z}_2)$  of two fermions, so that the sixteen  $U(4)$  density operators are then written as bilinear products of creation and annihilation operators as (the so called

Schwinger oscillator realization)

$$T_{\mu\nu} = \text{tr}(\mathcal{Z}^{\dagger} \tau_{\mu\nu} \mathcal{Z}), \quad \mathcal{Z} = \begin{pmatrix} \mathbf{a} \\ \mathbf{b} \end{pmatrix} = \begin{pmatrix} a_1^{\downarrow} & a_2^{\downarrow} \\ a_1^{\uparrow} & a_2^{\uparrow} \\ b_1^{\uparrow} & b_2^{\uparrow} \\ b_1^{\downarrow} & b_2^{\downarrow} \end{pmatrix}. \quad (1)$$

In the BLQH literature (see e.g. [3]) it is customary to denote the total spin  $S_k = T_{0k}/2$  and pseudospin  $P_k = T_{k0}/2$ , together with the remaining 9 isospin  $R_{kl} = T_{lk}/2$  operators for  $k, l = 1, 2, 3$ . A constraint in the Fock space of eight boson modes is imposed such that  $\mathcal{Z}^{\dagger} \mathcal{Z} = \lambda I_2$ , with  $\lambda$  representing the number of magnetic flux lines piercing each electron and  $I_2$  the  $2 \times 2$  identity. In particular, the linear Casimir operator  $T_{00} = \text{tr}(\mathcal{Z}^{\dagger} \mathcal{Z})$ , providing the total number of flux quanta, is fixed to  $n_a + n_b = \lambda + \lambda = 2\lambda$ , with  $n_a = n_{a1}^{\uparrow} + n_{a1}^{\downarrow} + n_{a2}^{\uparrow} + n_{a2}^{\downarrow}$  the total number of flux quanta in layer  $a$  (resp. in layer  $b$ ). The quadratic Casimir operator is also fixed to

$$\vec{S}^2 + \vec{P}^2 + \mathbf{R}^2 = \lambda(\lambda + 4). \quad (2)$$

We also identify the interlayer imbalance operator  $P_3$ , which measures the excess of flux quanta between layers  $a$  and  $b$ , that is  $\frac{1}{2}(n_a - n_b)$ . Therefore, the realization (1) defines a unitary bosonic representation of the  $U(4)$  matrix generators  $\tau_{\mu\nu}$  in the Fock space with constraints. This unitary irreducible representation arises in the Clebsch-Gordan decomposition of a tensor product of  $2\lambda$  four-dimensional (fundamental, elementary) representations of  $U(4)$ ; for example, in Young tableau notation:

$$\overbrace{\square \otimes \dots \otimes \square}^{2\lambda} = \overbrace{\begin{array}{|c|c|c|} \hline & & \lambda \\ \hline \dots & & \\ \hline \dots & & \\ \hline \end{array}}^{\lambda} \oplus \dots, \quad (3)$$

or  $\overbrace{[1] \otimes \dots \otimes [1]}^{2\lambda} = [\lambda, \lambda] \oplus \dots$ , where we wanted to highlight rectangular Young tableaux of shapes  $[\lambda, \lambda]$  (2 rows of  $\lambda$  boxes each) corresponding to 2 electrons pierced by  $\lambda$  magnetic flux lines (i.e., fractional filling factor  $\nu = 2/\lambda$ ). These are the Young tableaux determining our carrier Hilbert space  $\mathcal{H}_{\lambda}(\mathbb{G}_2^4)$  associated to the eight-dimensional Grassmannian phase spaces  $\mathbb{G}_2^4 = U(4)/U(2) \times U(2)$  (see [26–28] for similar pictures in  $N$ -component antiferromagnets). The dimension of this representation can be calculated by the hook-length formula and gives

$$d_{\lambda} = \frac{1}{12}(\lambda + 1)(\lambda + 2)^2(\lambda + 3) \quad (4)$$

In references [22, 25] we have also provided a physical argument to derive the expression of  $d_{\lambda}$  in a composite fermion picture. It turns out to coincide with the total number of ways to distribute  $2\lambda$  flux quanta among two identical electrons in four (spin-pseudospin) states. Note that quantum states associated to Young tableaux  $[\lambda, \lambda]$  are antisymmetric (fermionic character) under the interchange of the two electrons (two rows) for  $\lambda$  odd, whereas

they are symmetric (bosonic character) for  $\lambda$  even. Composite fermions require then  $\lambda$  odd.

In Refs. [22, 23] we have worked out an orthonormal basis of the carrier Hilbert space  $\mathcal{H}_\lambda(\mathbb{G}_2)$ , which is spanned by the set of orthonormal basis vectors

$$\left\{ |j, m\rangle_{q_a, q_b}, \quad 2j, m \in \mathbb{N}, \quad q_a, q_b = -j, \dots, j \right\}_{2j+m \leq \lambda}, \quad (5)$$

which can be written in terms of Fock states (to be self-contained, we give a brief in Appendix A). The basis states  $|j, m\rangle_{q_a, q_b}$  turn out to be antisymmetric (resp. symmetric) under the interchange of the two electrons for  $\lambda$  odd (resp. even), so that the parity of the number of flux quanta attached to each electron affects the quantum statistics of the compound (see [23]). The  $d_1 = 6$ -dimensional irrep of  $SU(4)$  is usually divided into two sectors (see e.g. [3]): the spin sector with spin-triplet pseudospin-singlet states

$$|\mathfrak{S}_\uparrow\rangle = \left| \frac{1}{2}, \frac{0}{\frac{1}{2}, \frac{1}{2}} \right\rangle, |\mathfrak{S}_0\rangle = \frac{1}{\sqrt{2}} \left( \left| \frac{1}{2}, \frac{0}{\frac{1}{2}, \frac{1}{2}} \right\rangle - \left| \frac{1}{2}, \frac{0}{\frac{-1}{2}, \frac{-1}{2}} \right\rangle \right), |\mathfrak{S}_\downarrow\rangle = \left| \frac{1}{2}, \frac{0}{\frac{1}{2}, \frac{-1}{2}} \right\rangle \quad (6)$$

and the ppin sector with pseudospin-triplet spin-singlet states

$$|\mathfrak{P}_\uparrow\rangle = \left| \frac{0, 1}{0, 0} \right\rangle, |\mathfrak{P}_0\rangle = \frac{1}{\sqrt{2}} \left( \left| \frac{1}{2}, \frac{0}{\frac{1}{2}, \frac{1}{2}} \right\rangle + \left| \frac{1}{2}, \frac{0}{\frac{-1}{2}, \frac{-1}{2}} \right\rangle \right), |\mathfrak{P}_\downarrow\rangle = \left| \frac{0, 0}{0, 0} \right\rangle. \quad (7)$$

The basis states  $|j, m\rangle_{q_a, q_b}$  are eigenstates of the following operators:

$$\begin{aligned} P_3 |j, m\rangle_{q_a, q_b} &= (2j + 2m - \lambda) |j, m\rangle_{q_a, q_b}, \\ (\vec{S}_a^2 + \vec{S}_b^2) |j, m\rangle_{q_a, q_b} &= 2j(j+1) |j, m\rangle_{q_a, q_b}, \\ S_{\ell 3} |j, m\rangle_{q_a, q_b} &= q_\ell |j, m\rangle_{q_a, q_b}, \quad \ell = a, b, \end{aligned} \quad (8)$$

where we have defined angular momentum operators in layers  $a$  and  $b$  as  $S_{ak} = -\frac{1}{2}(S_k + R_{k3})$  and  $S_{bk} = \frac{1}{2}(S_k - R_{k3})$ , respectively, so that  $\vec{S}_a^2 + \vec{S}_b^2 = \frac{1}{2}(\vec{S}^2 + \vec{R}^2)$ . Therefore,  $j$  represents the total angular momentum of layers  $a$  and  $b$ , whereas  $q_a$  and  $q_b$  are the corresponding third components. The integer  $m$  is related to the interlayer imbalance (ppin third component  $P_3$ ) through  $\frac{1}{2}(n_a - n_b) = (2j + 2m - \lambda)$ ; thus,  $m = \lambda, j = 0$  means  $n_a = 2\lambda$  (i.e., all flux quanta occupying layer  $a$ ), whereas  $m = 0, j = 0$  means  $n_b = 2\lambda$  (i.e., all flux quanta occupying layer  $b$ ). The angular momentum third components  $q_a, q_b$  measure the imbalance between spin up and down in each layer, more precisely,  $q_a = \frac{1}{2}(n_{a1}^\uparrow - n_{a1}^\downarrow + n_{a2}^\uparrow - n_{a2}^\downarrow)$  and similarly for  $q_b$ . For later use, we shall also provide the matrix elements of the interlayer tunneling operator

$$\begin{aligned} P_1 |j, m\rangle_{q_a, q_b} &= C_{q_a, q_b}^{j, m+1} |j - \frac{1}{2}, m+1\rangle_{q_a - \frac{1}{2}, q_b - \frac{1}{2}} + C_{-q_a, -q_b}^{j, m+1} |j - \frac{1}{2}, m+1\rangle_{q_a + \frac{1}{2}, q_b + \frac{1}{2}} + \\ &C_{-q_a + \frac{1}{2}, -q_b + \frac{1}{2}}^{j + \frac{1}{2}, m+2j+2} |j + \frac{1}{2}, m\rangle_{q_a - \frac{1}{2}, q_b - \frac{1}{2}} + C_{q_a + \frac{1}{2}, q_b + \frac{1}{2}}^{j + \frac{1}{2}, m+2j+2} |j + \frac{1}{2}, m\rangle_{q_a + \frac{1}{2}, q_b + \frac{1}{2}} + \\ &C_{q_a, q_b}^{j, m+2j+1} |j - \frac{1}{2}, m\rangle_{q_a - \frac{1}{2}, q_b - \frac{1}{2}} + C_{-q_a + \frac{1}{2}, -q_b + \frac{1}{2}}^{j + \frac{1}{2}, m} |j + \frac{1}{2}, m-1\rangle_{q_a - \frac{1}{2}, q_b - \frac{1}{2}} + \\ &C_{-q_a, -q_b}^{j, m+2j+1} |j - \frac{1}{2}, m\rangle_{q_a + \frac{1}{2}, q_b + \frac{1}{2}} + C_{q_a + \frac{1}{2}, q_b + \frac{1}{2}}^{j + \frac{1}{2}, m} |j + \frac{1}{2}, m-1\rangle_{q_a + \frac{1}{2}, q_b + \frac{1}{2}}, \quad (9) \end{aligned}$$

where the coefficients  $C$  were calculated in [22] and are given by

$$C_{q_a, q_b}^{j, m} = \frac{1}{2} \frac{\sqrt{(j+q_a)(j+q_b)m(\lambda - (m-2))}}{\sqrt{2j(2j+1)}}, \quad j \neq 0, \quad (10)$$

and  $C_{q_a, q_b}^{j, m} = 0$  for  $j = 0$ .

### III. MODEL HAMILTONIAN AND SEMICLASSICAL ANALYSIS

The total Landau-site Hamiltonian governing the bilayer QH system consists of Coulomb and a combination of Zeeman and pseudo-Zeeman interactions [1]

$$H = H_C + H_{ZpZ}. \quad (11)$$

In particular, we are just interested in the Hamiltonian reproducing the ground state energy which, for  $\nu = 2$  gives (we discard  $SU(4)$ -invariant terms)

$$H_C = 4\varepsilon_D^- P_3^2 - 2\varepsilon_X^- (\vec{S}^2 + \vec{R}_3^2 + P_3^2), \quad (12)$$

as a sum of the naive capacitance ( $\varepsilon_D^-$ ) and the exchange ( $\varepsilon_X^-$ ) interactions. The exchange and capacitance energy gaps are given in terms of the interlayer distance  $\delta$  by

$$\varepsilon_X^\pm = \frac{1}{4} \sqrt{\frac{\pi}{2}} \left( 1 \pm e^{(\delta/\ell_B)^2/2} \operatorname{erfc} \left( \frac{\delta}{\sqrt{2}\ell_B} \right) \right) \mathcal{E}_C, \quad (13)$$

and  $\varepsilon_D^- = \frac{\delta}{4\ell_B} \mathcal{E}_C$ , where  $\mathcal{E}_C = e^2/(4\pi\epsilon\ell_B)$  is the Coulomb energy unit and  $\ell_B = \sqrt{\hbar c/(eB)}$  the magnetic length. In the following we shall simply put  $\varepsilon_X^- = \varepsilon_X$  and  $\varepsilon_D^- = \varepsilon_D$  as no confusion will arise. We shall usually choose  $\delta = \ell_B$ , which gives  $\varepsilon_X \simeq 0.15$  in Coulomb units.

The (pseudo) Zeeman part

$$H_{ZpZ} = -\Delta_Z S_3 - \Delta_t P_1 - \Delta_b P_3 \quad (14)$$

is comprised of: Zeeman ( $\Delta_Z$ ), interlayer tunneling ( $\Delta_t$ , also denoted by  $\Delta_{\text{SAS}}$  in the literature [3]) and bias ( $\Delta_b$ ) gaps. The bias term creates an imbalanced configuration. For the sake of simplicity, we shall restrict ourselves to the balanced case in the semiclassical study, which eventually means to discard the terms proportional to  $\varepsilon_D$  and  $\Delta_b$ ; we shall take capacitance and bias into account in the quantum analysis of section IV.

A minimization process of the ground state energy surface (based on a semiclassical analysis) reveals the existence of three quantum phases: spin, canted and pseudospin (ppin for short), which are characterized by the squared spin  $\langle \vec{S} \rangle^2$  and ppin  $\langle \vec{P} \rangle^2$  ground state mean values (order parameters), as in figure 1 and table I for  $\lambda = 1$ . The spin (resp. ppin) phase occurs when the Zeeman (resp. tunneling) term dominates (see figure 1). The variational ground state energies of the three phases

Phase:	Spin	Ppin	Canted
Order	$\langle \vec{S} \rangle^2 = \lambda^2$	$\langle \vec{S} \rangle^2 = 0$	$\langle \vec{S} \rangle^2 \neq 0$
parameter:	$\langle \vec{P} \rangle^2 = 0$	$\langle \vec{P} \rangle^2 = \lambda^2$	$\langle \vec{P} \rangle^2 \neq 0$

TABLE I: Spin and ppin ground state mean values in the three BLQH phases.

(spin, canted and ppin) are given by the following expressions (see [1]; we write  $\Delta_{\text{SAS}} = \Delta_t$  for the sake of shortness)

$$\begin{aligned}
E_s &= -2\varepsilon_X - \Delta_Z, \\
E_c &= -2\varepsilon_X \left( \frac{1}{4} \frac{\Delta_t^2}{(2\varepsilon_X)^2} - \frac{1}{4} \frac{\Delta_Z^2}{(2\varepsilon_X)^2} + \frac{\Delta_t^2}{\Delta_t^2 - \Delta_Z^2} \right), \\
E_p &= -\Delta_t,
\end{aligned} \tag{15}$$

respectively, with second order QPT critical points at  $\Delta_t^{\text{sc}} = \sqrt{\Delta_Z^2 + 4\varepsilon_X \Delta_Z}$  (where  $E_s = E_c$  and  $\frac{\partial E_s}{\partial \Delta_t} = \frac{\partial E_c}{\partial \Delta_t}$ ) and  $\Delta_t^{\text{cp}} = 2\varepsilon_X + \sqrt{\Delta_Z^2 + 4\varepsilon_X^2}$  (where  $E_c = E_p$  and  $\frac{\partial E_c}{\partial \Delta_t} = \frac{\partial E_p}{\partial \Delta_t}$ ).

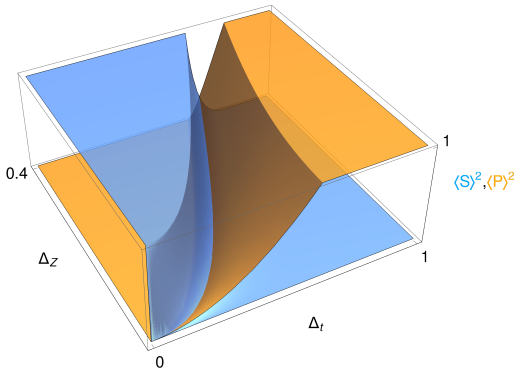


FIG. 1: Semiclassical expectation values of squared spin (blue) and ppin (orange) for  $\lambda = 1$  and layer separation  $\delta = \ell_B$ , as a function of tunneling  $\Delta_t$  and Zeeman  $\Delta_Z$  gaps (balanced case). We observe the three phases in table I. Coulomb energy units.

Let us see how this phase diagram is modified for fractional filling factors  $\nu = 2/\lambda$ . We have now  $N = 2\lambda$  bosonic particles (flux quanta), and therefore Coulomb (two-body) interactions must be renormalized by the number of pairs  $N(N-1)$  to make them intensive quantities. We also divide one-body interactions by  $N$  in order to work with energy density, as we are also interested in the large isospin  $\lambda \rightarrow \infty$  limit. Taking all this information into account, we propose the following Hamiltonian to study the ground state at fractional filling factors  $\nu = 2/\lambda$ :

$$H_\lambda = \frac{H_C}{N(N-1)} + \frac{H_{ZpZ}}{N}, \quad N = 2\lambda, \tag{16}$$

which is an adaptation of (11) to arbitrary  $N$  flux quanta (note that  $H_1 = H/2$ ). To study the semiclassical limit,

we now replace the operators  $P_j, S_j$  and  $R_{ij}$  by their expectation values  $\langle T_{\mu\nu} \rangle = \langle Z | T_{\mu\nu} | Z \rangle$  in a isospin- $\lambda$  coherent state  $|Z\rangle$  (see Appendix B) labeled by points  $Z \in \mathbb{G}_2^4$ , i.e.,  $2 \times 2$  complex matrices with four complex (eight real) entries denoted by  $z^\mu = \text{tr}(Z\sigma_\mu)/2, \mu = 0, 1, 2, 3$ . Let us define  $M_{\mu\nu} = 2i\lambda \frac{z_\mu \bar{z}^\nu - z_\nu \bar{z}^\mu}{\det(\sigma_0 + Z^\dagger Z)}$ , where  $z_\mu = \eta_{\mu\nu} z^\nu$  [we are using Einstein summation convention with Minkowskian metric  $\eta_{\mu\nu} = \text{diag}(1, -1, -1, -1)$ ] and  $\bar{z}^\mu$  is the complex conjugate. The coherent state expectation values of the operators appearing in the Hamiltonian (16) have the following expression (see Appendix B and references [22, 24] for their calculation)

$$\begin{aligned}
\langle S_1 \rangle &= M_{23}, \quad \langle S_2 \rangle = M_{31}, \quad \langle S_3 \rangle = M_{12}, \\
\langle R_{k3} \rangle &= iM_{0k}, \quad \langle \vec{S} \rangle^2 + \langle \vec{R}_3 \rangle^2 = M_{\mu\nu} M^{\mu\nu} / 2, \tag{17} \\
\langle P_1 \rangle &= \lambda \Re[\text{tr}(Z)(1 + \det(Z^\dagger)) / \det(\sigma_0 + Z Z^\dagger)], \\
\langle P_3 \rangle &= \lambda(\det(Z^\dagger Z) - 1) / \det(\sigma_0 + Z^\dagger Z),
\end{aligned}$$

where  $\Re$  denotes the real part [ $\langle P_2 \rangle$  corresponds to the imaginary part] and  $i$  is the imaginary unit. For the (cumbersome) coherent state expectation values of quadratic (two-body) operators  $\langle T^2 \rangle$  we address the reader to Refs. [22, 24]. Later we shall use a parametrization (B5) of  $Z$  in terms of eight angles, for which the imbalance expectation value is simply  $\langle P_3 \rangle = -(\cos \vartheta_+ + \cos \vartheta_-)/2$ . Note that the following identity for the magnitude of the  $SU(4)$  isospin is automatically fulfilled for coherent state expectation values:

$$\langle \vec{S} \rangle^2 + \langle \vec{P} \rangle^2 + \langle \mathbf{R} \rangle^2 = \lambda^2. \tag{18}$$

For  $\lambda = 1$  it coincides with the variational ground state condition provided in [1]. Note the difference with the expression of the quadratic Casimir (2), which is fulfilled for any state of the Hilbert space. The difference between both expressions denotes the existence of quantum fluctuations (non-zero variance) proportional to  $\lambda$  for the  $SU(4)$  isospin in a coherent state. These fluctuations are negligible (second order) in the large isospin,  $\lambda \rightarrow \infty$ , classical limit.

With these ingredients we can compute the energy surface  $E_\lambda(Z; \varepsilon_X, \Delta_t, \Delta_Z) = \langle Z | H_\lambda | Z \rangle$  and proceed to find the values of  $Z$  which minimize it. For this purpose, we have used the parametrization (B5) of  $Z$  in terms of eight angles (the dimension of the Grassmannian  $\mathbb{G}_2^4$ ). The results of the minimization are as follows. For arbitrary  $\lambda$ , we find the same phase diagram structure as for  $\lambda = 1$ , that is, spin, canted and ppin phases. In all phases we find the common relations

$$\beta_+ = \beta_- = 0, \quad \vartheta_+ + \vartheta_- = \pi, \quad \theta_a + \theta_b = \pi, \quad \phi_a = \phi_b. \tag{19}$$

In the spin and ppin phases we have

$$\text{Spin} : \vartheta_+^s = 0 = \theta_a^s, \quad \text{Ppin} : \vartheta_+^p = -\pi/2 = \theta_a^p, \tag{20}$$

respectively. In the canted phase we get the more in-

volved expression

$$\tan \vartheta_+^c = \pm \sqrt{\frac{(\Delta_t^2 - \Delta_Z^2)^2 - (4\Delta_Z \varepsilon_X(\lambda))^2}{-(\Delta_t^2 - \Delta_Z^2)^2 + (4\Delta_t \varepsilon_X(\lambda))^2}}, \quad (21)$$

$$\tan \theta_b^c = \mp \frac{\Delta_t}{\Delta_Z} \sqrt{\frac{(\Delta_t^2 - \Delta_Z^2)^2 - (4\Delta_Z \varepsilon_X(\lambda))^2}{-(\Delta_t^2 - \Delta_Z^2)^2 + (4\Delta_t \varepsilon_X(\lambda))^2}},$$

where we have defined  $\varepsilon_X(\lambda) = \lambda \varepsilon_X / (2\lambda - 1)$  for later use. Note that we have two different solutions of  $(\vartheta_+^c, \theta_b^c)$  in the canted phase, given by the signs  $(+, -)$  and  $(-, +)$  in equation (21), leading to the same minimum energy  $\langle Z_\pm^c | H_\lambda | Z_\pm^c \rangle$ , with  $Z_\pm^c = Z(\theta_{a,b}, \phi_{a,b}, \vartheta_\pm, \beta_\pm)|_\pm^c$  the corresponding stationary point in the Grassmannian  $\mathbb{G}_2^4$  for any of the two solutions  $(+) = (+, -)$  and  $(-) = (-, +)$  together with the common restrictions (19). Even though both coherent states  $|Z_+^c\rangle$  and  $|Z_-^c\rangle$  give the same energy, they are distinct; in fact, they are almost orthogonal  $\langle Z_+^c | Z_-^c \rangle \simeq 0$  in the canted phase. This indicates that the ground state is degenerated and there is a broken symmetry in the thermodynamic limit. We will come back to these degeneracy problems of the canted phase in the next section.

Let us denote collectively by  $Z_+^0$  and  $Z_-^0$  the two sets of stationary points in any of the three (spin, canted and ppin) quantum phases (note that  $Z_+^0 = Z_-^0$  in the spin and ppin phases). Both sets of stationary points provide the same value of the energy expectation value  $E_\lambda(Z_\pm^0; \varepsilon_X, \Delta_t, \Delta_Z) = \langle Z_\pm^0 | H_\lambda | Z_\pm^0 \rangle$ , which we shall simply denote by  $E_\lambda^0(\varepsilon_X, \Delta_t, \Delta_Z)$ . After some algebraic manipulations, one can see that  $E_\lambda^0$  coincides with (15) when replacing  $\varepsilon_X \rightarrow \varepsilon_X(\lambda)$ , except for a zero-point energy correction  $\mathcal{E}_\lambda^0 = -2\varepsilon_X / (2\lambda - 1)$ . This zero-point energy is just due to the non-zero quantum fluctuations  $\langle A^2 \rangle \neq \langle A \rangle^2$  of  $SU(4)$  operators [compare for example (2) with (18)] and it vanishes in the high isospin  $\lambda$  limit. There is also a normalization factor of two difference since, for  $\lambda = 1$ , the Hamiltonians (11) and (16) are related by  $H_1 = H/2$ . In Figure 2 we represent the variational energy density  $E_\lambda^0$  as a function of  $\Delta_t$  for  $\Delta_Z = 0.01$  and interlayer distance  $\delta = \ell_B$  for different values of  $\lambda$ . We see that the spin, canted and ppin phase regions (separated by vertical grid lines) are affected by the value of the isospin  $\lambda$ ; in fact, the new critical points are displaced at

$$\Delta_t^{\text{sc}}(\lambda) = \sqrt{\Delta_Z^2 + 4\varepsilon_X(\lambda)\Delta_Z}, \quad (22)$$

$$\Delta_t^{\text{cp}}(\lambda) = 2\varepsilon_X(\lambda) + \sqrt{\Delta_Z^2 + 4\varepsilon_X^2(\lambda)},$$

coinciding with the ones after eq. (15) when replacing  $\varepsilon_X \rightarrow \varepsilon_X(\lambda)$ . The high isospin limit,  $\lambda \rightarrow \infty$  is also straightforwardly accomplished just by replacing  $\varepsilon_X \rightarrow \varepsilon_X(\infty) = \varepsilon_X/2$  in the energy (15) and critical points  $\Delta_t^{\text{sc}}$  and  $\Delta_t^{\text{cp}}$ . We see that the width of the canted region  $\Delta_t^{\text{cp}}(\lambda) - \Delta_t^{\text{sc}}(\lambda)$  shrinks as  $\lambda$  increases. We also compare in figure 2 the variational (solid) and numerical (dashed) ground state energies (see next section for a quantum

analysis). We realize that the variational and numerical results coincide in the spin phase but not in the canted and ppin regions, except in the high isospin  $\lambda$  limit, where exact results converge to the semiclassical (mean-field) limit.

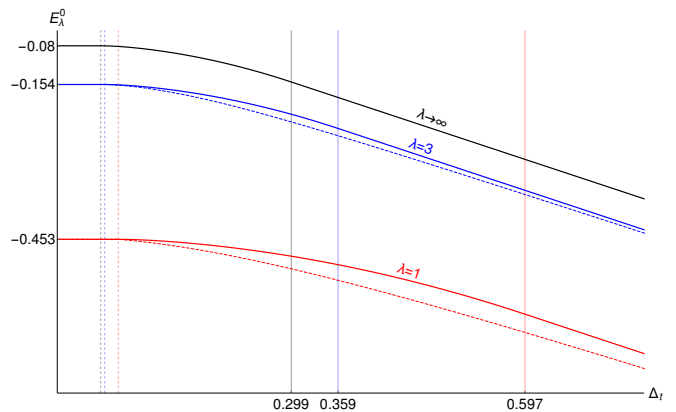


FIG. 2: Variational (solid) and exact (dotted) ground state energy  $E_\lambda^0$  as a function of tunneling  $\Delta_t$  (fixed layer separation  $\delta = \ell_B$  and Zeeman  $\Delta_Z = 0.01$ ) for  $\lambda = 1$  (red),  $\lambda = 3$  (blue) and  $\lambda \rightarrow \infty$  (dotted black). The corresponding spin-canted  $\Delta_t^{\text{sc}}(\lambda)$  and canted-ppin  $\Delta_t^{\text{cp}}(\lambda)$  phase transition points are represented by vertical dashed and solid grid lines, respectively. Numerical values for the canted-ppin transition points  $\Delta_t^{\text{cp}}(\lambda)$  are also indicated. For the spin-canted transition we have  $\Delta_t^{\text{sc}}(1) = 0.078$ ,  $\Delta_t^{\text{sc}}(3) = 0.061$  and  $\Delta_t^{\text{sc}}(\infty) = 0.056$ . Coulomb energy units.

Spin-canted and canted-ppin phase transition points are better appreciated in Figure 3, where we represent normalized squared spin  $\langle \vec{S} \rangle^2$  and ppin  $\langle \vec{P} \rangle^2$  order parameters for the variational coherent states  $|Z_\pm^0\rangle$  as a function of  $\Delta_t$  for  $\Delta_Z = 0.01$ ,  $\delta = \ell_B$  and different values of  $\lambda$ . An explicit expression of spin  $\langle \vec{S} \rangle^2$  and ppin  $\langle \vec{P} \rangle^2$  can be easily obtained from the expectation values (17), together with the restrictions (19) common to the three phases, resulting in

$$\langle \vec{S} \rangle^2 = \lambda^2 \cos^2 \vartheta_+ \cos^2 \theta_b,$$

$$\langle \vec{P} \rangle^2 = \lambda^2 \sin^2 \vartheta_+ \sin^2 \theta_b.$$

In the spin phase ( $\vartheta_+ = 0 = \theta_b$ ) we have maximum spin  $\langle \vec{S} \rangle^2 = \lambda^2$  [remember the identity (18)] and minimum ppin  $\langle \vec{P} \rangle^2 = 0$ , whereas in the ppin phase ( $\vartheta_+ = -\pi/2 = \theta_b$ ) we have minimum spin  $\langle \vec{S} \rangle^2 = 0$  and maximum ppin  $\langle \vec{P} \rangle^2 = \lambda^2$ . In the canted phase, when inserting (21) into (23), we realize that both spin and ppin do not attain the maximum value, as can be appreciated in figure 3 and summarized in table I [the case  $\lambda = 1$  was already depicted in figure 1]. Note that both (negative and positive) values of  $\theta_a^c$  and  $\vartheta_+^c$  in (21) give the same values of energy and squared spin and ppin in (23), even though the corresponding variational states  $|Z_-^c\rangle$  and  $|Z_+^c\rangle$  are different (quasi-orthogonal). This reflects a degeneracy problem that we shall analyze in the following section.

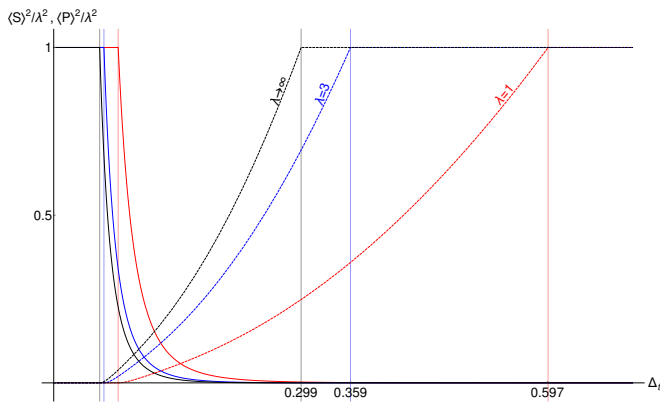


FIG. 3: Semiclassical expectation values of squared spin (solid) and ppin (dashed) for  $\lambda = 1$  (red),  $\lambda = 3$  (blue) and  $\lambda \rightarrow \infty$  (black) for layer separation  $\delta = \ell_B$  and  $\Delta_Z = 0.01$ , as a function of tunneling  $\Delta_t$ . Vertical grid lines indicate the spin-canted and canted-ppin (with numerical value) phase transition points for each  $\lambda$ . Coulomb energy units.

#### IV. QUANTUM ANALYSIS AND NUMERICAL DIAGONALIZATION RESULTS

In this section we solve the eigenvalue problem for the Hamiltonian (16) and compare with the mean field (semi-classical) results of the previous section, analyzing the effect of quantum fluctuations. The Hamiltonian matrix elements in the basis (5) are determined by the expressions (8) and (9). For example, for  $\lambda = 1$  and arranging the basis vectors (5) as

$$\begin{aligned} |1\rangle &= |0,0\rangle, |2\rangle = |0,1\rangle, |3\rangle = \left| \frac{1}{2}, \frac{0}{2} \right\rangle, \\ |4\rangle &= \left| \frac{1}{2}, \frac{0}{2} \right\rangle, |5\rangle = \left| \frac{1}{2}, \frac{0}{2} \right\rangle, |6\rangle = \left| \frac{1}{2}, \frac{0}{2} \right\rangle, \end{aligned} \quad (23)$$

we obtain the  $6 \times 6$  Hamiltonian matrix

$$H_1 = \begin{pmatrix} \frac{1}{2}(\Delta_b + 4\varepsilon_D - 2\varepsilon_X) & 0 & -\frac{\Delta_t}{4} & -\frac{\Delta_t}{4} & 0 & 0 \\ 0 & \frac{1}{2}(-\Delta_b + 4\varepsilon_D - 2\varepsilon_X) & -\frac{\Delta_t}{4} & -\frac{\Delta_t}{4} & 0 & 0 \\ -\frac{\Delta_t}{4} & -\frac{\Delta_t}{4} & -3\varepsilon_X & 0 & 0 & 0 \\ -\frac{\Delta_t}{4} & -\frac{\Delta_t}{4} & 0 & -3\varepsilon_X & 0 & 0 \\ 0 & 0 & 0 & 0 & -\frac{1}{2}(\Delta_Z + 6\varepsilon_X) & 0 \\ 0 & 0 & 0 & 0 & 0 & \frac{1}{2}(\Delta_Z - 6\varepsilon_X) \end{pmatrix} \quad (24)$$

Those readers more acquainted with the spin-triplet (ppin-singlet) and ppin-triplet (spin-singlet) states can perform the change of basis (6) and (7). The lowest (ground state) energy  $E_\lambda^0$  is plotted in figure 2 (dotted curves) as a function of  $\Delta_t$  for  $\lambda = 1$  and  $\lambda = 3$  (Hilbert space dimensions  $d_1 = 6$  and  $d_3 = 50$ , respectively). As we have already commented, the exact ground state energy coincides with the mean-field result in the spin phase. Actually, the lowest energy eigenstate in the spin phase is the basis state  $|j_a, m_a\rangle = |\lambda/2, 0\rangle$ , which is also a extremal case of coherent state  $|Z\rangle$  for the critical angle values (19) and (20) in the spin phase. The mean-field result does not coincide with the numerical diagonalization in the canted and ppin phases, but the energy difference between both gets smaller as  $\lambda$  increases, as can be appreciated in figure 2.

In figure 4 we represent the exact (red) variational (dotted-black) and parity-adapted (blue; see below) ground state squared expectation values of spin  $\langle \vec{S} \rangle^2$  (solid) and ppin  $\langle \vec{P} \rangle^2$  (dashed) as a function of  $\Delta_t$  for  $\lambda = 3$ . The variational case was already depicted in figure 3 and presents a smooth behavior, which contracts with the step-like behavior in the quantum case, mainly

in the canted phase, where we find in general  $\lambda$  steps for  $\langle \vec{S} \rangle^2$  and  $\langle \vec{P} \rangle^2$ . Moreover, the transition from canted to ppin phase is not so well marked as the transition from spin to canted phase, which occurs quite sharply. This result agrees with the one obtained in [6] through an exact diagonalization of a few-electron system, where the boundary between the spin and canted phases is practically unmodified from the mean-field result, but the boundary between the canted and ppin phases is considerably modified. The step-like behavior of spin and ppin in the canted phase is due to a level crossing at certain values of the tunneling  $\Delta_t$  for which the ground and first excited energy levels degenerate. The number of level crossings increases with  $\lambda$ , in fact, there are exactly  $\lambda$  crossings (see figure 5). In the high isospin  $\lambda$  limit, this might indicate that there is an avoided crossing in the whole canted region. This degenerate situation makes that the overlap between the variational (mean-field)  $|Z_\pm^0\rangle$  and exact (numerical)  $|\psi_\lambda^0\rangle$  ground states is quite small and irregular in the canted phase. We get better results (but still not good enough) by adapting our variational states to the parity symmetry, that is, by

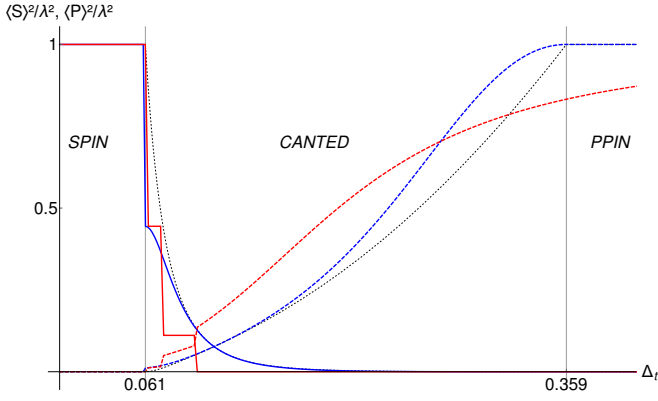


FIG. 4: Exact (red) variational (dotted-black) and parity-adapted (blue) ground state squared expectation values of spin  $\langle \vec{S} \rangle^2$  (solid) and ppin  $\langle \vec{P} \rangle^2$  (dashed) for  $\lambda = 3$ , layer separation  $\delta = \ell_B$  and  $\Delta_Z = 0.01$ , as a function of tunneling  $\Delta_t$ . Vertical grid lines indicate the spin-canted  $\Delta_t^{\text{sc}}(3) = 0.061$  and canted-ppin  $\Delta_t^{\text{cp}}(3) = 0.359$  phase transition points for  $\lambda = 3$ . Coulomb energy units.

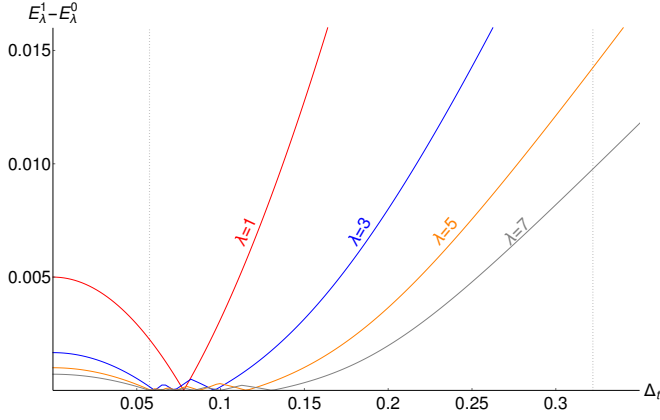


FIG. 5: Energy gap between ground and first energy levels as a function of  $\Delta_t$ , for  $\delta = \ell_B$ ,  $\Delta_Z = 0.01$  and different values of  $\lambda$ . Vertical grid lines indicate the spin-canted  $\Delta_t^{\text{sc}}(\infty) = 0.0556$  and canted-ppin  $\Delta_t^{\text{cp}}(\infty) = 0.299$  transition points for the limiting case  $\lambda \rightarrow \infty$ . Coulomb energy units.

taking the normalized symmetric combination

$$|Z_{\text{sym}}^0\rangle = \frac{|Z_+^0\rangle + |Z_-^0\rangle}{\sqrt{2(1 + \Re(\langle Z_+^0 | Z_-^0 \rangle))}}. \quad (25)$$

The results of the overlap/fidelity  $|\langle Z_{\text{sym}}^0 | \psi_\lambda^0 \rangle|^2$  between variational and exact ground states is shown in figure 6. We see that the fidelity is 1 in the spin phase (where the variational and exact ground states coincide with  $|\frac{\lambda/2}{-\lambda/2}, \frac{0}{\lambda/2}\rangle$ ) and less than 1 in the ppin phase (although it increases with  $\Delta_t$ ). The degenerate situation in the canted phase gives low fidelity, except for  $\lambda = 1$ . A fidelity drop is also expected at the phase

transition point, where quantum fluctuations dominate. For completeness, we have also represented in figure 4 the squared expectation values of spin  $\langle Z_{\text{sym}}^0 | \vec{S} | Z_{\text{sym}}^0 \rangle^2$  (solid-blue curve) and ppin  $\langle Z_{\text{sym}}^0 | \vec{P} | Z_{\text{sym}}^0 \rangle^2$  (dashed-blue) in the parity-adapted state (25), which ‘interpolates’ between the semiclassical and the quantum case.

Parity adapted coherent states like (25) have also been successfully used to better reproduce the exact quantum results at finite-size from the mean-field approximation in other interesting models undergoing a second order QPT like for example the Dicke model of atom-field interactions [30–32], the vibron model of molecules [33–36] and the Lipkin-Meshkov-Glick model [37].

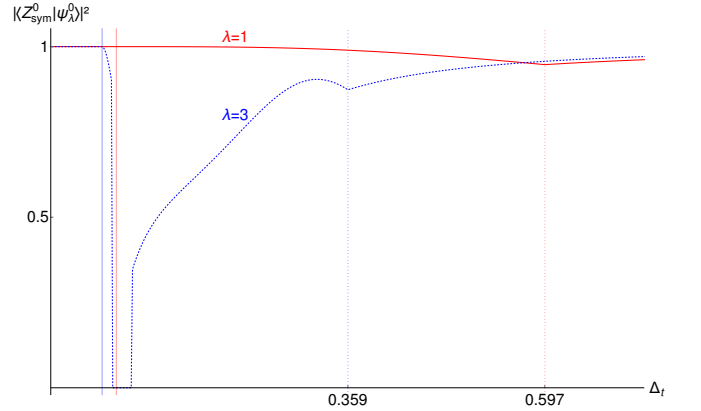


FIG. 6: Overlap/fidelity  $|\langle Z_{\text{sym}}^0 | \psi_\lambda^0 \rangle|^2$  between variational (coherent states) adapted to the parity symmetry and exact ground states, as a function of  $\Delta_t$ , for  $\delta = \ell_B$ ,  $\Delta_Z = 0.01$ ,  $\lambda = 1$  (red) and  $\lambda = 3$  (blue-dashed). Spin-canted and canted-ppin (with numerical value) phase transition points are indicated by vertical solid and dotted grid lines, respectively. Coulomb energy units.

So far we have only studied the balanced case and restricted our analysis to the ground (and first excited) state. For completeness, let us introduce imbalance (capacitive and bias terms) and have a look to the whole spectrum. In figure 7 we represent the energy spectrum as a function of  $\Delta_t$  for  $\lambda = 3$  (dimension  $d_3 = 50$ ).

For zero tunneling  $\Delta_t = 0$  (spin phase) we observe a band energy structure that we can explain as follows. The Hamiltonian for this case is diagonal in the basis (5) and the corresponding eigenvalues can be straightforwardly obtained from (8) as

$$E_{\lambda(q_a, q_b)}^{(j, m)} = \frac{\varepsilon_{\text{cap}}(2j + m - \lambda)^2 - 8\varepsilon_X j(j + 1)}{2\lambda(2\lambda - 1)} - \frac{\Delta_Z(q_b - q_a) + \Delta_b(2j + 2m - \lambda)}{2\lambda}, \quad (26)$$

where  $\varepsilon_{\text{cap}} = 4\varepsilon_D - 2\varepsilon_X$  denotes the capacitance energy. For small Zeeman and bias interactions, the dominant part are the capacitance and exchange energies which grow with the squared angular momentum

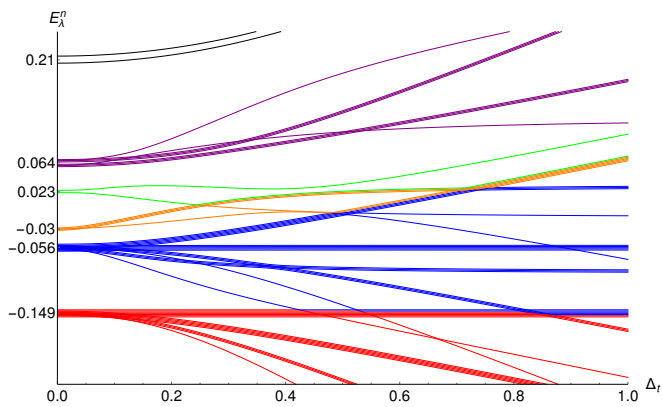


FIG. 7: Energy spectrum as a function of  $\Delta_t$ , for  $\delta = \ell_B$ ,  $\Delta_Z = 0.01$ ,  $\Delta_b = 0.01$  and  $\lambda = 3$ . The six energy bands emerge in the spin phase (small  $\Delta_t$ ). They are plotted in different colors and its structure is given in table II. Coulomb energy units.

$E_\lambda^{j,\varsigma}$	$j, \varsigma$	No. levels
-0.15	$j = 3/2, \varsigma = 0$	16
-0.056	$j = 1, \varsigma = 1$	18
-0.03	$j = 1/2, \varsigma = 0$	4
0.023	$j = 0, \varsigma = 1$	2
0.064	$j = 1/2, \varsigma = 2$	8
0.21	$j = 0, \varsigma = 3$	2
	Total:	50

TABLE II: Representative value of the band energy  $E_\lambda^{j,\varsigma}$  at  $\Delta_t = 0$  (spin phase) for  $\lambda = 3$  and  $\Delta_Z = 0.01 = \Delta_b$ . Each energy band ( $j, \varsigma$ ) is roughly determined by angular momentum and layer population imbalance  $\varsigma = |2j + 2m - \lambda|$ . There are  $2(2j + 1)^2$  closely spaced energy levels forming each energy band ( $j, \varsigma$ ), except for  $\varsigma = 0$ , where there are only  $(2j + 1)^2$ . Coulomb energy units.

$j(j + 1)$  and the squared layer population imbalance  $\varsigma^2 = (2j + 2m - \lambda)^2$ . These two magnitudes ( $j, \varsigma$ ) roughly determine (with some exceptions for higher  $\lambda$ ) the energy band arrangement at zero tunneling. In table II we represent the band energy structure, giving a representative value of the band energy  $E_\lambda^{j,\varsigma}$  together with the values of the angular momentum  $j$  and absolute imbalance  $\varsigma = |2j + 2m - \lambda|$  common to each energy band for  $\lambda = 3$ . In general, there are two values of  $m_\pm = (\pm\varsigma + \lambda - 2j)/2$  and  $(2j + 1)^2$  values of  $q_a, q_b$  common to every couple ( $j, \varsigma$ ), so that the total number of levels forming the energy band ( $j, \varsigma$ ) is  $2(2j + 1)^2$ , except for  $\varsigma = 0$  that is just  $(2j + 1)^2$ . Small bias and Zeeman interactions slightly break the degeneracy in  $m$  and  $q_a, q_b$ , respectively, determining the bandwidth.

For large tunneling  $\Delta_t$  (ppin phase), energy bands are formed around the eigenvalues of the ppin first component  $P_1$ , that is, at energies about  $E_\lambda^{j+m} = -\Delta_t(2j +$

$2m - \lambda)/(2\lambda)$ , since the eigenvalues of  $P_1$  and  $P_3$  coincide (actually, the discussion also applies for large bias voltage). Therefore, the number of energy bands arising at high  $\Delta_t$  is exactly  $2\lambda + 1$  [remember discussion in paragraph between (8) and (9)]. We can label each band by  $n = 2j + 2m$  [the homogeneity degree of polynomials (A2)] and the number of closely spaced energy levels forming each energy band  $n$  is

$$D_n = \begin{cases} \frac{(n+1)(n+2)(n+3)}{6}, & n \leq \lambda, \\ \frac{(2\lambda-n+1)(2\lambda-n+2)(2\lambda-n+3)}{6}, & \lambda \leq n \leq 2\lambda. \end{cases} \quad (27)$$

One can verify that  $\sum_{n=0}^{2\lambda} D_n = d_\lambda$  gives the dimension of the Hilbert space. At intermediate tunneling (canted phase) there is an intricate spectrum structure with multiple band-crossing.

## V. CONCLUSIONS AND OUTLOOK

The physics of multicomponent quantum Hall systems, and particularly the bilayer case, is very rich. The fractional case incorporates extra ingredients that makes the problem even much more interesting. In this article we have analyzed the bilayer (four components) case at fractional values  $\nu = 2/\lambda$  of the filling factor. We have obtained the phase diagram structure of the balanced case by using an overcomplete set of coherent (semiclassical) variational states previously introduced. The Hamiltonian used is an adaptation of the integer case,  $\nu = 2$ , to an arbitrary number of magnetic flux quanta  $\lambda$  per electron, to make it intensive and to study the large  $SU(4)$ -isospin  $\lambda$  limit. Up to our knowledge, an study of this type has not been done before. We have also performed a numerical diagonalization of the Hamiltonian and compared exact (quantum) with mean-field (semiclassical) results for the ground state. The accordance is quite good in the spin and ppin phases, but not in the canted phase, where degeneracies and energy level crossings occur, specially at large  $\lambda$ . We have also analyzed the full energy spectrum and we have found an energy band arrangement in spin and ppin phases. The particular structure of these energy bands has also been analyzed in terms of angular momentum and layer population imbalance quantum numbers. An experimental corroboration of these band energy formation would enforce our theoretical work. To finish, just to say that a generalization of the previous study to arbitrary  $N$  component quantum Hall systems at fractional filling factors  $\nu = M/\lambda$  could also be (in principle) carried out with the help of our recent construction of  $U(N)/[U(M) \times U(N - M)]$  coherent states [25] (this is still work in progress).

## Acknowledgements

The work was supported by the Spanish project FIS2014-59386-P (MINECO and FEDER funds). C.

Peón-Nieto acknowledges the research contract with Ref. 4537 financed by the project above.

### Appendix A: Orthonormal basis for arbitrary $\lambda$

In Refs. [22, 23] we have provided a Fock space representation of the BLQH basis states (5) for fractional filling factor  $\nu = 2/\lambda$ . The general expression is given by the action of creation operators  $\mathbf{a}^\dagger$  and  $\mathbf{b}^\dagger$  in layers  $a$  and  $b$  [see (1) for the definition of  $2 \times 2$  matrix annihilation operators  $\mathbf{a}$  and  $\mathbf{b}$ ] acting on the Fock vacuum  $|0\rangle_F$  as

$$|j, m\rangle_{q_a, q_b} = \frac{1}{\sqrt{2j+1}} \sum_{q=-j}^j (-1)^{q_a-q} \quad (A1)$$

$$\times \frac{\varphi_{-q, -q_a}^{j, m}(\mathbf{a}^\dagger) \varphi_{q, q_b}^{j, \lambda-2j-m}(\mathbf{b}^\dagger)}{\sqrt{\frac{\lambda!(\lambda+1)!}{(\lambda-2j-m)!(\lambda+1-m)!}} \sqrt{\frac{\lambda!(\lambda+1)!}{m!(2j+m+1)!}}} |0\rangle_F,$$

where

$$\varphi_{q_a, q_b}^{j, m}(Z) = \sqrt{\frac{2j+1}{\lambda+1} \binom{\lambda+1}{2j+m+1} \binom{\lambda+1}{m}} \quad (A2)$$

$$\times \det(Z)^m \mathcal{D}_{q_a, q_b}^j(Z), \quad 2j+m \leq \lambda, \quad q_a, q_b = -j, \dots, j,$$

are homogeneous polynomials of degree  $2j+2m$  in four complex variables arranged in a  $2 \times 2$  complex matrix  $Z = (z_{kl})$ . Here

$$\mathcal{D}_{q_a, q_b}^j(Z) = \sqrt{\frac{(j+q_a)!(j-q_a)!}{(j+q_b)!(j-q_b)!}} \sum_{k=\max(0, q_a+q_b)}^{\min(j+q_a, j+q_b)} \quad (A3)$$

$$\binom{j+q_b}{k} \binom{j-q_b}{k-q_a-q_b} z_{11}^k z_{12}^{j+q_a-k} z_{21}^{j+q_b-k} z_{22}^{k-q_a-q_b},$$

denotes the usual Wigner  $\mathcal{D}$ -matrix [39] with angular momentum  $j$ . The set of polynomials (A2) verifies the closure relation

$$\sum_{m=0}^{\lambda} \sum_{j=0; \frac{1}{2}}^{(\lambda-m)/2} \sum_{q_a, q_b=-j}^j \overline{\varphi_{q_a, q_b}^{j, m}(Z')} \varphi_{q_a, q_b}^{j, m}(Z) = K_\lambda(Z'^\dagger, Z),$$

with  $K_\lambda(Z'^\dagger, Z) = \det(\sigma_0 + Z'^\dagger Z)^\lambda$  the so called Bergmann kernel.

### Appendix B: Coherent states on $\mathbb{G}_2^4$

An overcomplete set of coherent states for  $\nu = 2/\lambda$  has been worked out in Ref. [22]. Coherent states  $|Z\rangle$  are labeled by a  $2 \times 2$  complex matrix  $Z$  (a point on the Grassmannian  $\mathbb{G}_2^4$ ) and can be expanded in terms of the orthonormal basis vectors (A1) as

$$|Z\rangle = \frac{\sum_{m=0}^{\lambda} \sum_{j=0; \frac{1}{2}}^{(\lambda-m)/2} \sum_{q_a, q_b=-j}^j \varphi_{q_a, q_b}^{j, m}(Z) |j, m\rangle_{q_a, q_b}}{\det(\sigma_0 + Z^\dagger Z)^{\lambda/2}}, \quad (B1)$$

with coefficients  $\varphi_{q_a, q_b}^{j, m}(Z)$  in (A2). They can also be written in the form of a boson condensate as (see [22])

$$|Z\rangle = \frac{1}{\lambda! \sqrt{\lambda+1}} \left( \frac{\det(\check{\mathbf{b}}^\dagger + Z^t \check{\mathbf{a}}^\dagger)}{\sqrt{\det(\sigma_0 + Z^\dagger Z)}} \right)^\lambda |0\rangle_F, \quad (B2)$$

where  $\check{\mathbf{a}}^\dagger = \frac{1}{2} \eta^{\mu\nu} \text{tr}(\sigma_\mu \mathbf{a}^\dagger) \sigma_\nu$  denotes the ‘‘parity reversed’’  $2 \times 2$ -matrix creation operator of  $\mathbf{a}^\dagger$  in layer  $a$  (similar for layer  $b$ ) [we are using Einstein summation convention with Minkowskian metric  $\eta_{\mu\nu} = \text{diag}(1, -1, -1, -1)$ ]. Coherent states are normalized,  $\langle Z|Z\rangle = 1$ , but they do not constitute an orthogonal set since they have a non-zero (in general) overlap given by

$$\langle Z'|Z\rangle = \frac{K_\lambda(Z'^\dagger, Z)}{K_{\lambda/2}(Z'^\dagger, Z') K_{\lambda/2}(Z^\dagger, Z)} \quad (B3)$$

Sometimes it is useful to use a coherent state picture (Bargmann-Fock representation) of a general state  $|\psi\rangle$  given by  $\Psi(Z) \equiv K_{\lambda/2}(Z, Z') \langle Z|\psi\rangle$ . For example, the Bargmann-Fock representation of the basis states  $|j, m\rangle_{q_a, q_b}$  is given by the homogeneous polynomials  $\varphi_{q_a, q_b}^{j, m}(Z)$  in (A2). Given a  $U(4)$  group element (written in block matrix form)

$$U = \begin{pmatrix} A & B \\ C & D \end{pmatrix}, \quad A, B, C, D \in \text{Mat}(2, \mathbb{C}),$$

a point  $Z$  in the Grassmannian  $\mathbb{G}_2^4 = U(4)/U(2)^2$  can be identified with  $Z = BD^{-1}$  in the chart where  $D$  is invertible. From the composition law of two group elements  $U'' = U'U$  we get the (Möbius-like) transformation  $Z' = B''D''^{-1} = (A'Z + B')(C'Z + D')^{-1}$  of  $Z$  under a group translation  $U'$ . This transformation also defines a representation of the  $U(4)$  infinitesimal generators  $\tau_{\mu\nu}$  on the space of holomorphic functions  $\Psi(Z)$ , given in terms of differential operators  $\mathcal{T}_{\mu\nu}$  in four complex coordinates  $z^\mu = \text{tr}(Z\sigma_\mu)/2, \mu = 0, 1, 2, 3$ . For example, it is easy to see that the differential realization of the imbalance ppin generator  $\tau_{k0}/2$  is given by  $\mathcal{P}_3 = z^\mu \partial_\mu - \lambda$ , where we use the Einstein summation convention and denote  $\partial_\mu = \partial/\partial z^\mu$  and  $z_\nu = \eta_{\nu\mu} z^\mu$ , with  $\eta_{\nu\mu} = \text{diag}(1, -1, -1, -1)$  the Minkowskian metric. In addition, spin  $\mathcal{S}_k$  and  $\mathcal{R}_{k3}$  are written in terms of  $\mathcal{M}_{\mu\nu} = z_\mu \partial_\nu - z_\nu \partial_\mu$  as  $\mathcal{S}_i = \frac{1}{2} \epsilon^{ikl} \mathcal{M}_{kl}$  and  $\mathcal{R}_{k3} = M_{k0}$ , respectively, where  $\epsilon^{ikl}$  is the totally antisymmetric tensor (see [22, 24] for the remainder  $\mathcal{T}_{\mu\nu}$  operators). With this differential realization, the (cumbersome) computation of expectation values of operators in a coherent state (usually related to order parameters) is reduced to the (easy) calculation of derivatives of the Bergmann kernel as:

$$\langle Z|T_{\mu\nu}|Z\rangle = K_\lambda^{-1}(Z, Z') \mathcal{T}_{\mu\nu} K_\lambda(Z, Z'). \quad (B4)$$

We have used this simple formula to compute the expectation values (17).

To finish this appendix, let us introduce a parametrization of  $Z$  in terms of eight angles  $\theta_{a,b}, \vartheta_{\pm} \in [0, \pi)$  and  $\phi_{a,b}, \beta_{\pm} \in [0, 2\pi)$ , given by the following decomposition

$$Z = V_a \begin{pmatrix} \xi_+ & 0 \\ 0 & \xi_- \end{pmatrix} V_b^\dagger, \quad \xi_{\pm} = \tan \frac{\vartheta_{\pm}}{2} e^{i\beta_{\pm}},$$

$$V_\ell = \begin{pmatrix} \cos \frac{\theta_\ell}{2} & -\sin \frac{\theta_\ell}{2} e^{i\phi_\ell} \\ \sin \frac{\theta_\ell}{2} e^{-i\phi_\ell} & \cos \frac{\theta_\ell}{2} \end{pmatrix}, \quad \ell = a, b, \quad (\text{B5})$$

where  $V_{a,b}$  represent rotations in layers  $\ell = a, b$  (note their ‘‘conjugated’’ character). This parametrization of  $Z$  has been useful to minimize the energy surface  $\langle Z|H_\lambda|Z \rangle$  for the Hamiltonian (16).

- 
- [1] Z.F. Ezawa, M. Eliashvili, G. Tsitsishvili, Ground-state structure in  $\nu = 2$  bilayer quantum Hall systems. *Phys. Rev. B* **71** (2005) 125318
- [2] J.K. Jain, Composite fermions, Cambridge University Press, New York, 2007.
- [3] Z. F. Ezawa, Quantum Hall Effects: Field Theoretical Approach and Related Topics (2nd Edition), World Scientific 2008
- [4] A. H. MacDonald, R. Rajaraman and T. Jungwirth, Broken-symmetry ground states in  $\nu = 2$  bilayer quantum Hall systems, *Phys. Rev. B* **60**, 8817 (1999)
- [5] L. Brey, E. Demler and S. Das Sarma, Electromodulation of the Bilayered  $\nu = 2$  Quantum Hall Phase Diagram, *Phys. Rev. Lett.* **83** (1999) 168-171
- [6] J. Schliemann A. H. MacDonald, Bilayer Quantum Hall Systems at Filling Factor  $\nu = 2$ : An Exact Diagonalization Study, *Phys. Rev. Lett.* **84** (2000) 4437.
- [7] K. Hasebe and Z. F. Ezawa, Grassmannian fields and doubly enhanced Skyrmions in the bilayer quantum Hall system at  $\nu = 2$ , *Phys. Rev. B* **66**, 155318 (2002)
- [8] A. Fukuda et al., Magnetotransport study of the canted antiferromagnetic phase in bilayer  $\nu = 2$  quantum Hall state. *Phys. Rev. B* **73** (2006) 165304
- [9] L. Zheng, R. Radtke, and S. Das Sarma, Spin-Excitation-Instability-Induced Quantum Phase Transitions in Double-Layer Quantum Hall Systems, *Phys. Rev. Lett.* **78**, 2453 (1997).
- [10] S. Das Sarma, S. Sachdev, and L. Zheng, Double-Layer Quantum Hall Antiferromagnetism at Filling Fraction  $\nu = 2/m$  where  $m$  is an Odd Integer, *Phys. Rev. Lett.* **79**, 917 (1997); Canted antiferromagnetic and spin-singlet quantum Hall states in double-layer systems, *Phys. Rev. B* **58**, 4672 (1998).
- [11] Ajit C. Balram, Csaba Toke, A. Wójs and J. K. Jain, Phase diagram of fractional quantum Hall effect of composite fermions in multicomponent systems, *Phys. Rev. B* **91**, 045109 (2015)
- [12] M. O. Goerbig and N. Regnault, Analysis of a SU(4) generalization of Halperin’s wave function as an approach towards a SU(4) fractional quantum Hall effect in graphene sheets, *Phys. Rev. B* **75**, 241405(R) (2007)
- [13] K. Yang, S. Das Sarma and A.H. MacDonald, Collective modes and skyrmion excitations in graphene SU(4) quantum Hall ferromagnets, *Phys. Rev. B* **74**, 075423 (2006)
- [14] C.R. Dean et al., Multicomponent fractional quantum Hall effect in graphene, *Nature Physics* **7** (2011) 693-696
- [15] Y. Zheng, A. Sawada, Z. F. Ezawa, Theoretical approach to ground states of the  $\nu = 2/3$  bilayer fractional quantum Hall systems. *Solid State Communications* **115** (2013) 82-87
- [16] N. Kumada et al., Phase Diagram of Interacting Composite Fermions in the Bilayer  $\nu = 2/3$  Quantum Hall Effect, *Phys. Rev. Lett.* **89** (2002) 116802
- [17] N. Kumada et al., Phase diagrams of  $\nu = 2$  and  $\nu = 2/3$  quantum Hall states in bilayer systems, *Phys. Rev. B* **69** (2004) 155319
- [18] R.B. Laughlin, Anomalous Quantum Hall Effect: An Incompressible Quantum Fluid with Fractionally Charged Excitations, *Phys. Rev. Lett.* **50** (1983) 1395-1398
- [19] B.I. Halperin, Statistics of quasiparticles and the hierarchy of fractional quantized hall states, *Phys. Rev. Lett.* **52** (1984) 1583-1586.
- [20] F.D.M. Haldane, Fractional Quantization of the Hall Effect: A Hierarchy of Incompressible Quantum Fluid States, *Phys. Rev. Lett.* **51** (1983) 605-608
- [21] A.H. MacDonald, G.C. Aers and M.W.C. Dharma-wardana, Hierarchy of plasmas for fractional quantum Hall states, *Physical Review B*. **31** (1985) 5529
- [22] M. Calixto and E. Pérez-Romero, Coherent states on the Grassmannian  $U(4)/U(2)^2$ : Oscillator realization and bilayer fractional quantum Hall systems, *J. Phys. A: Math. Theor.* **47**, (2014) 115302.  
Erratum: there is a misprint in equation (49) of this reference. One must replace  $C_{:,2j+m+1}$  by  $C_{:,2j+m+2}$ .
- [23] M. Calixto and E. Pérez-Romero, Interlayer coherence and entanglement in bilayer quantum Hall states at filling factor  $\nu = 2/\lambda$ , *J. Phys.: Condens. Matter* **26** (2014) 485005
- [24] M. Calixto and E. Pérez-Romero, Some properties of Grassmannian  $U(4)/U(2)^2$  coherent states and an entropic conjecture, *J. Phys. A: Math. Theor.* **48** (2015) 495304
- [25] M. Calixto, C. Peón-Nieto and E. Pérez-Romero, Coherent states for N-component fractional quantum Hall systems and their nonlinear sigma models, *Annals of Physics* **373** (2016) 52-66
- [26] I. Affleck, The quantum Hall effects,  $\sigma$ -models at  $\theta = \pi$  and quantum spin chains, *Nucl. Phys.* **B257** (1985) 397; I. Affleck, Exact critical exponents for quantum spin chains, non-linear  $\sigma$ -models at  $\theta = \pi$  and the quantum hall effect, **B265** (1986) 409-447; I. Affleck, Critical behaviour of SU(n) quantum chains and topological non-linear  $\sigma$ -models, *Nucl. Phys.* **B305** (1988), 582-596
- [27] N. Read and S. Sachdev, Some features of the phase diagram of the square lattice SU(N) antiferromagnet, *Nucl. Phys.* **B316** (1989) 609
- [28] D. P. Arovas, A. Karlhede and D. Lilliehöök, SU(N) quantum Hall skyrmions, *Phys. Rev.* **B59** (1999) 13147-

- 13150.
- [29] R. Gilmore, The Classical Limit Of Quantum Nonspin Systems, *J. Math. Phys.* 20 (1979) 891-893
- [30] O. Castaños, E. Nahmad-Achar, R. López-Peña, and J. G. Hirsch, Superradiant phase in field-matter interactions, *Phys. Rev. A*, 84 013819 (2011). Erratum *Phys. Rev. A* 84, 049901(E) (2011)
- [31] M. Calixto, A. Nagy, I. Paradela and E. Romera, Signatures of quantum fluctuations in the Dicke model by means of Renyi uncertainty, *Phys. Rev. A* 85 (2012) 053813.
- [32] E. Romera, R. del Real and M. Calixto, Husimi distribution and phase-space analysis of a Dicke-model quantum phase transition, *Phys. Rev. A* 85 (2012) 053831.
- [33] F. Perez-Bernal and F. Iachello, Algebraic approach to two-dimensional systems: Shape phase transitions, monodromy, and thermodynamic quantities, *Phys. Rev. A* 77, 032115 (2008).
- [34] M. Calixto, R. del Real and E. Romera, Husimi distribution and phase-space analysis of a vibron-model quantum phase transition, *Phys. Rev. A* 86, 032508 (2012).
- [35] M. Calixto, E. Romera and R. del Real, Parity-symmetry-adapted coherent states and entanglement in quantum phase transitions of vibron models, *J. Phys. A: Math. Theor.* 45 (2012) 365301 (12pp).
- [36] M. Calixto and F. Perez-Bernal, Entanglement in shape phase transitions of coupled molecular bendings, *Phys. Rev. A* 89, 032126 (2014)
- [37] E. Romera, M. Calixto and O. Castaños, Phase space analysis of first, second and third-order quantum phase transitions in the Lipkin-Meshkov-Glick model, *Phys. Scr.* 89 (2014) 095103 (14pp)
- [38] G. Dev and J. K. Jain, Band Structure of the Fractional Quantum Hall Effect, *Phys. Rev. Lett.* 69 (1992) 2843-2846
- [39] L.C. Biedenharn, J.D. Louck, *Angular Momentum in Quantum Physics*, Addison-Wesley, Reading, MA, 1981; L.C. Biedenharn, J.D. Louck, *The Racah-Wigner Algebra in Quantum Theory*, Addison-Wesley, New York, MA 1981